SAND2015-9037J

Large On-Chip Amplification in Silicon via Forward Stimulated Brillouin Scattering

Eric A. Kittlaus, Heedeuk Shin, and Peter T. Rakich
Department of Applied Physics, Yale University, New Haven, CT 06520 USA.
(Dated: October 15, 2015)

Strong Brillouin coupling has only recently been realized in silicon using a new class of optomechanical waveguides that yield both optical and phononic confinement. Despite these major advances, appreciable Brillouin amplification has yet to be observed in silicon. Using new membrane-suspended silicon waveguide we report large Brillouin amplification for the first time, reaching levels greater than 5 dB for modest pump powers, and demonstrate a record low (5 mW) threshold for net amplification. This work represents a crucial advance necessary to realize high-performance Brillouin lasers and amplifiers in silicon.

Both Kerr and Raman nonlinearities are radically enhanced by tight optical-mode confinement in nanoscale silicon waveguides [1–4]. Counter-intuitively, Brillouin nonlinearities are exceedingly weak in these same nonlinear waveguides [5]. Only recently have strong Brillouin interactions been realized in a new class of optomechanical structures that control the interaction between guided photons and phonons [5–7]. With careful design, such Brillouin nonlinearities over-take all other nonlinear processes in silicon[6, 7]; these same Brillouin interactions are remarkably tailorable, permitting a range of hybrid photonic-phononic signal processing operations that have no analog in all-optical signal processing[8–12]. Using this physics, the rapidly growing field of silicon-based Brillouin-photonics has produced new frequency agile RF-photonic notch filters[8, 10, 13, 14] and multipole bandpass filters[12] as the basis for radio-frequency photonic (RF-photonic) signal processing. Beyond these specific examples, the potential impact of such Brillouin interactions is immense; frequency combs[13, 15, 16], ultra-low phase-noise lasers[17–19], sensors[9, 12, 20], optical isolation[21–23], and an array signal processing technologies[8, 12–14, 24, 25] may be possible in silicon with further progress.

However, strong Brillouin amplification–essential to many new Brillouin-based technologies–has yet to be realized in silicon photonics. Despite the creation of strong Brillouin nonlinearities in a range of new structures[6, 7], nonlinear losses and free carrier effects have stifled attempts to demonstrate net optical amplification. Only recently, Van Laer *et al.* reported modest 0.5 dB (12%) amplification [26] using suspended silicon nanowire structures of the type proposed in Ref. [5]. However, sensitivity to surface imperfections challenges the robustness of this system. Furthermore, Brillouin nonlinearities diminish with longer interaction lengths due to inhomogeneous broadening. Careful theoretical analyses by Wolff *et al.*, suggest that large net amplification is fundamentally challenging to achieve in such silicon nanowires at near-IR wavelengths [27].

In this paper, we report large Brillouin amplification in silicon for the first time through an alternative device paridigm; using an all-silicon membrane structure (Fig. 1) that permits independent design of photonic and phononic modes, we demonstrate net amplification at remarkably low (< 5 mW) pump powers, and record-high amplification (5.2 dB) at 60 mW powers. These results represents a 30-fold improvement in amplification over prior systems [26]. In contrast to Ref. [6], this *all-silicon* system yields a combination of a large Brillouin gain ($G_B > 10^3\,\mathrm{W^{-1}m^{-1}}$) and record-low propagation losses ($< 0.2\,\mathrm{dB\ cm^{-1}}$) permitting 40 times larger nonlinear interactions. Using such strong couplings, we demonstrate cascaded-Brillouin energy transfer in a silicon waveguide for the first time. In addition to new silicon-based Brillouin laser technologies, this new regime of Brillouin coupling opens the door for nonreciprocal signal processing schemes and comb generation.

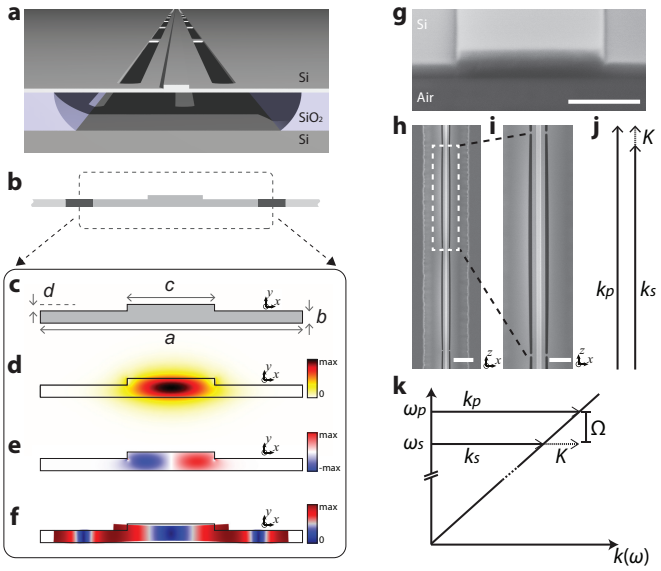

FIG. 1. Hybrid photonic-phononic silicon waveguide. (a) schematic of continuously suspended silicon Brillouin-active waveguide and (b) cross-section of the active region. (c) diagram showing critical device dimensions. (c), (d), and (f) are E_x field of guided optical mode, x-component of electrostrictive body force, and the elastic displacement field of the Brillouin active phonon mode, respectively. (g) cross-sectional SEM of waveguide core, while (h) and (i) show top-down SEM images of fabricated device. Scale bars indicate 500 nm, 10 μm and 5 μm in (g), (h), and (i) respectively. Phase-matching diagram of (j) is shown atop optical dispersion relation in (k).

This Brillouin-active waveguide system is continuously suspended over centimeter-lengths by a series nanoscale tethers, as seen in Fig. 1a. The active region of the suspended waveguide (Fig. 1b) is diagrammed in Fig. 1c. Light is confined to the central ridge structure through total-internal reflection, which supports guidance of the low-loss TE-like guided optical mode at $\lambda = 1550$ nm (Fig. 1d). Figure 1e shows the electrostrictive optical force distribution generated by this mode; these optical forces mediate efficient coupling to the guided phonon mode (Fig. 1f) at GHz frequencies. Confinement of this guided phonon mode (Fig. 1f) is produced by the large acoustic impedance mismatch between silicon and air.

Co-propagating pump and Stokes waves of frequencies ω_p and ω_s are guided in the same TE-like optical mode and couple through parametrically generated acoustic phonons with frequency $\Omega_B = \omega_p - \omega_s$. Coupling is mediated by guided phonon modes that satisfy the phase matching condition $K(\Omega_B) = k(\omega_p) - k(\omega_s)$ sketched in Fig 1j-k, where $K(\Omega)$ and $k(\omega)$ are the acoustic and optical dispersion relations. In the forward scattering case, phase matching requires $K(\Omega_B) \cong (\Omega_B/v_g)$, where $v_g \equiv (\partial\omega/\partial k)$ is the group velocity of the optical mode. Hence, phonons which mediate forward-SBS have a vanishing longitudinal wave-vector. As described in Ref. [6], a set of guided acoustic waves (or Lamb-waves) with exceedingly low (<1 m/s) group velocities satisfy this condition. The underlying dynamics of this process is similar to that first observed in optical fibers [15], permitting both signal amplification and cascaded energy transfer that is distinct in nature from the more widely studied backwards-SBS process [28].

These devices are fabricated from a crystalline silicon layer through a silicon-on-insulator (SOI) fabrication process (see Methods). Scanning electron micrographs of the device cross-section and top-down view are shown in Fig. 1g and Fig. 1h-i respectively. The device consists of 1 μm wide ridge that sits atop a 3 μm wide, 160 nm thick silicon membrane. Each suspended region (seen in Fig. 1i) is supported by symmetrically placed nanoscale tethers spaced every 50 μm along the waveguide length; this design enables robust fabrication of several centimeter long Brillouin-active waveguides. Note that the supporting tethers have negligible contribution to the optical losses. In what follows, we examine Brillouin interactions in a 29 mm long continuously suspended Brillouin active device comprised of 570 suspended segments.

Direct measurements of the Brillouin gain were performed using the apparatus of Fig. 2a. Figures 2b.i-iii show the forward-Brillouin gain spectra for pump-wave powers of 21, 36, and 62 mW respectively. These spectra reveal a high quality-factor ($Q = 680$) Brillouin resonance at 4.35 GHz, demonstrating remarkable robustness to dimensional variations. Figure 2e shows the peak Brillouin gain as a function of pump power, reaching a maximum value of 6.9 dB at the highest (62 mW) pump power, consistent with a Brillouin gain coefficient of $G_b = 1152 \pm 54$ W^{-1}m^{-1}. Independent measurements

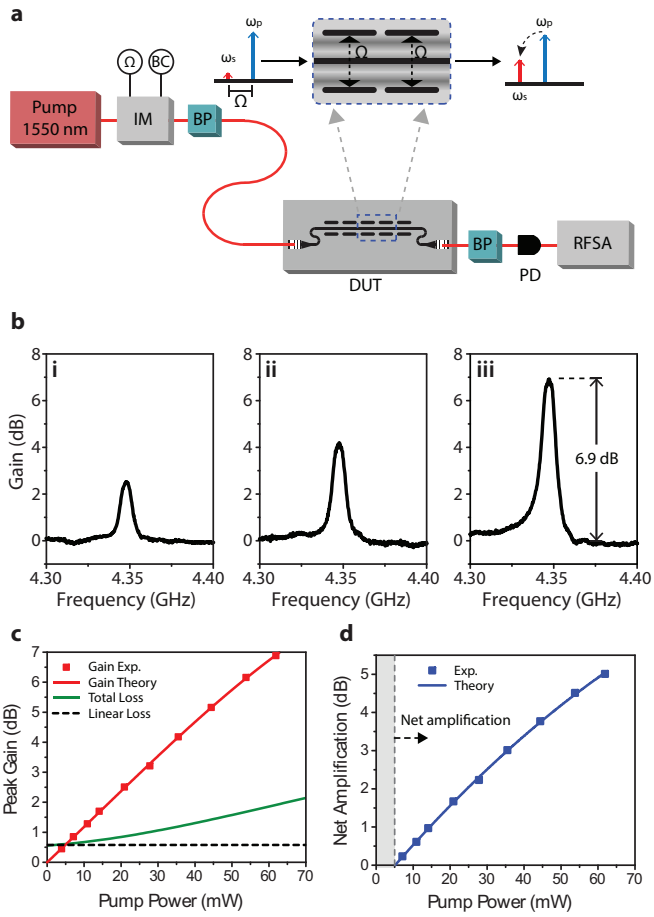

FIG. 2. Experimental results showing Brillouin gain and net amplification. (a) Diagram of the experimental apparatus; abbreviations detailed in Methods. Panels i, ii, and iii of (b) are the Brillouin gain spectra obtained for powers 21, 36, and 62 mW respectively. (c) plots peak gain (red), linear loss (dash) and total loss (green) versus pump power at 1550 nm wavelengths. (d) Net amplification as a function of pump power. The threshold for amplification is 5 mW.

performed through heterodyne four-wave mixing spectroscopy yield a value of $G_B = 1117 \pm 176$ W^{-1}m^{-1} (see Supplementary Information). Both measurements show good agreement with calculated frequency, 4.41 GHz, and Brillouin gain 1015 ± 193 W^{-1}m^{-1} from a finite element simulation.

The net Brillouin amplification (Fig. 2f) is obtained by subtracting the total loss (green) from the peak Brillouin gain (red) in Fig. 2e. These data reveal a peak on-chip amplification of 5.2 dB at 62 mW powers; moreover, the threshold for net amplification occurs at record-low (< 5 mW) optical powers owing to the low propagation losses and large Brillouin gain coefficient of this system. Note that the total waveguide loss represents the sum of the linear and nonlinear waveguide losses. Through these measurements, net amplification (5.2 dB) was limited only by the power handling of the tapered input couplers; amplification continues to grow at the highest

pump powers (62 mW). Hence further amplification is clearly achievable with improved input coupler designs.

This large nonlinear coupling also enables cascaded forward-Brillouin energy transfer. This interaction, previously only observed in highly nonlinear microstructured fibers [15], is quantified by injecting two drive fields at frequencies ω_0 and ω_1 into the Brillouin-active waveguide. Nonlinear coupling between these equal intensity drive fields, with frequency separation Ω_B, produce resonant phonon-mediated energy transfer (Fig. 3a). Heterodyne spectral analysis is used to quantify cascaded energy transfer to successive Stokes and anti-Stokes orders, of frequencies $\{\omega_l\}$, at the device output; three characteristic spectra are shown in Fig. 3b-d, corresponding to injected powers $P = P_0 = P_1$ of 0.1 mW, 13 mW and 32 mW respectively. These data reveal 62% power transfer from $l=1$ to $l=\{-2,-1,0,+2,+3\}$ orders through strong light driven acousto-optic energy transfer.

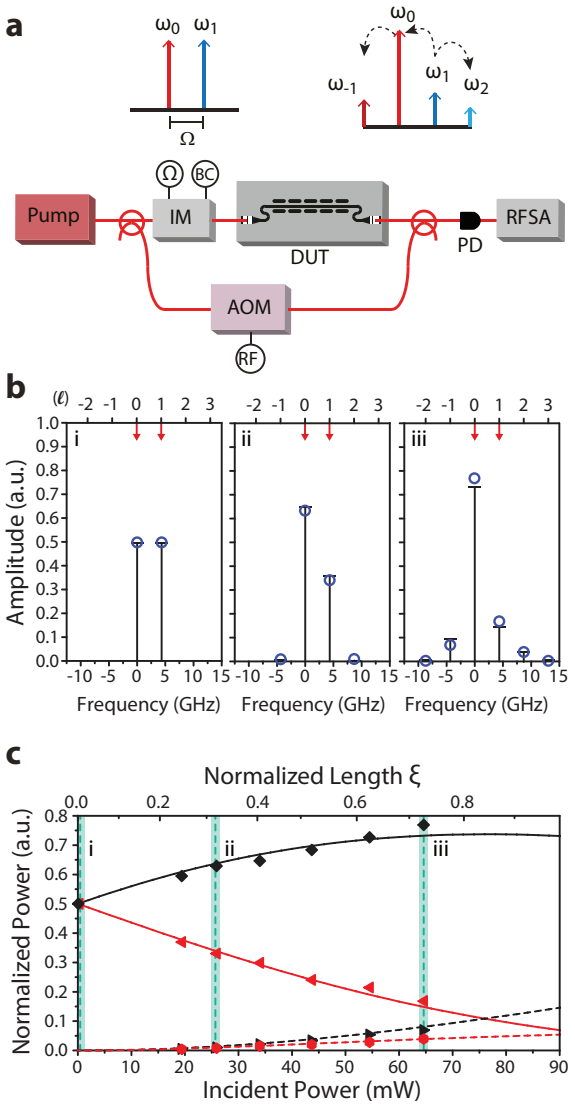

FIG. 3. Setup and results of an energy transfer (two-tone) experiment (a) Experimental diagram to measure power transfer driven by two pump fields of equal magnitude (b) Frequency power spectrum of output light as a function of total on-chip power. (c) Power transfer as a function of on-chip power showing theoretical calculations (lines) and measured amplitudes for pump fields ω_0 and ω_1 (solid black, solid red) and first cascaded fields ω_{-1} and ω_2 (solid red, dashed red) fields. The vertical blue lines correspond to panels i-iii above.

This cascading process is unique to forward Brillouin scattering; through this process the cascaded optical fields coherently drive the same phonon field producing successive parametric frequency shifts [15]. The relevant figure of merit for cascaded energy transfer is the power-gain-length product ξ, which is defined as $\xi \equiv G_B\sqrt{(P_0 P_1)}L_{eff} = G_B P L_{eff}$. Here, L_{eff} is the effective interaction length taking into account nonlinear loss (see Supplementary Information). At the highest tested power, this device admits a normalized propagation length $\xi = 0.71$. As seen from both experiment and theory in Fig. 3c, the demonstrated coupling strength approach maximal depletion of the ω_1 drive-field, resulting in significant energy transfer to higher order Stokes and anti-Stokes orders. This process is a basis for wideband nonreciprocal energy transfer, comb generation, and waveform synthesis [15].

More generally, the realization of numerous Brillouin laser and amplifier technologies hinge upon relative strength the Brillouin coupling and linear/nonlinear losses. In this regard, this planar waveguide topology offers several advantages over nanowire systems. Greatly reduced sensitivity of this optical mode to lithographic sidewall roughness permits ultra-low (0.18 ± 0.02 dB cm^{-1}) propagation losses [29, 30], enabling interaction lengths of 25 cm, more than an order of magnitude larger than prior systems [6, 7, 26]. In addition, this same waveguide geometry drastically shortens the effective free-carrier lifetimes (~ 2 ns) relative to bulk (> 10 ns) through rapid in-plane diffusion of carriers [31]. Short free carrier lifetimes, combined with a reduced TPA coefficient, result in 15-times lower nonlinear losses than the nanowire systems analyzed in Ref. [27]. Together these properties yield an unprecedented Brillouin gain figure of merit of $\mathscr{F} = 5.2$ [27]. (For further details see Supplement.) Hence, this unique hybrid photonic-phononic waveguide design represents a significant advance over prior silicon nanowire waveguide systems. Moreover, this improved figure of merit suggests significant opportunity for high-efficiency Brillouin amplification and cascaded energy transfer.

Thus far, we have focused on individual Brillouin-active waveguides of 2.9 cm length, and the injected optical powers have been limited to ~ 60 mW by the input coupling method. With high power input couplers, this waveguide geometry readily supports guided powers of 150 mW [12]. Furthermore, low propagation losses permit exceptionally large (25 cm) propagation lengths. Taking nonlinear losses into account, these conditions would enable 30 dB of amplification over a 20 cm waveg-

uide length; a cascaded energy transfer figure of merit of $\xi \cong 3.8$ is also achieved under these conditions, corresponding to efficient energy transfer to more than 20 comb lines. However, this level of performance is only possible if inhomogeneous broadending does not diminish the Brillouin gain along the device length [6, 7, 26].

To explore the impact of inhomogeneous broadening on Brillouin gain, we studied devices with lengths from 500 microns to 2.9 cm (for details see Supplement). The shortest waveguide lengths reveal gains of $G_B = 1837 \pm 134\ \mathrm{W^{-1}m^{-1}}$; this increased gain is consistent with measured higher effective phononic Q-factors ($Q \cong 1019 \pm 59$). As lengths are increased (L = 0.5, 2.5, 5 and 29 mm) the Q-factor and gain monatonically decrease in a manner consistent with inhomogeneous broadening. Note however, the majority of dimensionally induced broadening occurs over the first 5 milimeters. Only a marginal (15%) increase in linewidth is seen for a 6-fold increase in length (i.e., from 0.5 cm to 2.9 cm), demonstrating a greatly improved net Brillouin amplification with increasing device length.

These results contrast sharply with recent studies of nanowire waveguides [6, 7, 26]. To understand why, we analyze the sensitivity of Brillouin frequency with dimensional variations. FEM simulations reveal resonant frequency changes of $1.4\,\mathrm{MHz\,nm^{-1}}$, $0.8\,\mathrm{MHz\,nm^{-1}}$, and $0.7\,\mathrm{MHz\,nm^{-1}}$ with variations in device dimensions a, b, and c, as diagrammed in Fig. 1c. (see Supplementary information for full details.) This degree of dimensional sensitivity is 10 times smaller than that of nanowire systems ($19\,\mathrm{MHz\,nm^{-1}}$) [7], which explains the improved robustness and scalability of this system.

To explore the potential for higher single-pass amplification, we also fabricated Brillouin-active waveguide structures with lengths up to 8.7 cm. These structures (consisting of 1,710 suspended segments) produced reliable low-loss optical transmission. However, for lengths greater than 2.9 cm it was necessary to wrap the waveguide using a serpentine device geometry. This change in layout also altered the character of the resonance lineshape, suggesting that systematic effects (e.g., proximity effect, stress propagation, and process variations) likely play a role in excess broadening observed in these modified device designs. Hence, to approach the theoretical limits of Brillouin gain and nonlinear coupling described above, it may be necessary to implement systematic frequency compensation across fabricated devices.

Nevertheless, the demonstrated Brillouin amplification and improved figures of merit already open the door to high performance Brillouin laser and signal processing technologies. For instance, the ultra low ($0.18 \pm 0.02\ \mathrm{dB\,cm^{-1}}$) propagation losses of this waveguide geometry translate to optical cavity Q-factors of > 4 million. Using this new waveguide design, efficient and tailorable all-silicon Brillouin lasers are readily achieved with threshold powers approaching 10 mW.

In summary, using a new suspended ridge waveguide system, with independent photonic and phononic tailorability, we have demonstrated large Brillion amplification necessary to achieve high-performance on-chip Brillouin lasers and signal processing technologies. The device's large nonlinear figure of merit is enabled by excellent linear and nonlinear loss performance of the membrane structure. Net amplification of over 5 dB is demonstrated for modest (60 mW) pump powers . The device also exhibits significant cascaded energy transfer mediated by a single phonon field. Analysis of Brillouin gain and device performance demonstrates that there is in fact immense potential for flexible silicon-based Brillouin photonics at near-IR wavelengths. This combination of high nonlinearity with robust optical and acoustic performance opens the door for a wide range of hybrid silicon photonic-phononic technologies for RF and photonic signal processing, waveform and pulse synthesis, optical isolators and filtering, and new light sources.

1. Fabrication Methods

The silicon waveguides were written on a silicon-on-insulator chip with a 3 μm oxide layer using electron beam lithography on hydrogen silsesquioxane photoresist. Following development, a Cl_2 reactive ion etch was employed to etch the ridge waveguide structure. After a solvent cleaning step, slots were written to expose the oxide layer, again with electron beam lithography of ZEP520A photoresist and Cl_2 RIE. The device was then wet released via a 49% hydrofluoric acid etch of the oxide undercladding.

2. Experimental Methods

Both experiments used a pump laser operating around 1550 nm. Light is coupled in and out of the waveguide through the use of grating couplers with measured coupling losses of 6.5 dB. For the gain experiment, the band pass filters are used to ensure that only fields ω_p and ω_s are injected and measured. The following abbreviations are used in the experimental diagrams:

Fig. 2a: IM Mach-Zehnder intensity modulator, BC DC bias controller, BP band-pass filter, DUT device under test, PD photodetector, RFSA radio frequency spectrum analyzer.

Fig. 3a: IM Mach-Zehnder intensity modulator, BC DC bias controller, AOM acousto-optic modulator, DUT device under test, PD photodetector, RFSA radio frequency spectrum analyzer.

3. Acknowledgements

This work was supported by the MesoDynamic Architectures program at DARPA under the direction of Dr. Daniel Green. We thank Prashanta Kharel for technical

discussions involving phononic systems and nonlinear interactions. We are grateful to Dr. Ryan Behunin, Dr. William Renninger, and Dr. Whitney Purvis Rakich for careful reading and critique of this manuscript.

[1] H. Rong, A. Liu, R. Nicolaescu, M. Paniccia, O. Cohen, and D. Hak, Applied Physics Letters **85** (2004).
[2] H. Rong, R. Jones, A. Liu, O. Cohen, D. Hak, A. Fang, and M. Paniccia, Nature **433**, 725 (2005).
[3] B. Jalali, V. Raghunathan, R. Shori, S. Fathpour, D. Dimitropoulos, and O. Stafsudd, Selected Topics in Quantum Electronics, IEEE Journal of **12**, 1618 (2006).
[4] M. A. Foster, A. C. Turner, J. E. Sharping, B. S. Schmidt, M. Lipson, and A. L. Gaeta, Nature **441**, 960 (2006).
[5] P. T. Rakich, C. Reinke, R. Camacho, P. Davids, and Z. Wang, Phys. Rev. X **2**, 011008 (2012).
[6] H. Shin, W. Qiu, R. Jarecki, J. A. Cox, R. H. Olsson, A. Starbuck, Z. Wang, and P. T. Rakich, Nat Commun **4** (2013).
[7] R. Van Laer, B. Kuyken, D. Van Thourhout, and R. Baets, Nat Photon **9**, 199 (2015).
[8] B. Vidal, M. A. Piqueras, and J. Martí, Opt. Lett. **32**, 23 (2007).
[9] M. Li, W. H. P. Pernice, C. Xiong, T. Baehr-Jones, M. Hochberg, and H. X. Tang, Nature **456**, 480 (2008).
[10] W. Zhang and R. Minasian, Photonics Technology Letters, IEEE **24**, 1182 (2012).
[11] R. Pant, D. Marpaung, I. V. Kabakova, B. Morrison, C. G. Poulton, and B. J. Eggleton, Laser & Photonics Reviews **8**, 653 (2014).
[12] H. Shin, J. A. Cox, R. Jarecki, A. Starbuck, Z. Wang, and P. T. Rakich, Nat Commun **6** (2015).
[13] J. Li, H. Lee, and K. J. Vahala, Nat Commun **4** (2013).
[14] D. Marpaung, B. Morrison, M. Pagani, R. Pant, D.-Y. Choi, B. Luther-Davies, S. J. Madden, and B. J. Eggleton, Optica **2**, 76 (2015).
[15] M. S. Kang, A. Nazarkin, A. Brenn, and P. S. J. Russell, Nat Phys **5**, 276 (2009).
[16] D. Braje, L. Hollberg, and S. Diddams, Phys. Rev. Lett. **102**, 193902 (2009).
[17] N. Olsson and J. van der Ziel, Electronics Letters **22**, 488 (1986).
[18] K. S. Abedin, P. S. Westbrook, J. W. Nicholson, J. Porque, T. Kremp, and X. Liu, Opt. Lett. **37**, 605 (2012).
[19] J. Li, H. Lee, and K. J. Vahala, Opt. Lett. **39**, 287 (2014).
[20] F. Gao, R. Pant, E. Li, C. G. Poulton, D.-Y. Choi, S. J. Madden, B. Luther-Davies, and B. J. Eggleton, Opt. Express **21**, 8605 (2013).
[21] Z. Yu and S. Fan, Nat Photon **3**, 91 (2009).
[22] M. S. Kang, A. Butsch, and P. S. J. Russell, Nat Photon **5**, 549 (2011).
[23] X. Huang and S. Fan, Lightwave Technology, Journal of **29**, 2267 (2011).
[24] X. Yao, Photonics Technology Letters, IEEE **10**, 138 (1998).
[25] A. Loayssa, D. Benito, and M. J. Garde, Opt. Lett. **25**, 1234 (2000).
[26] R. Van Laer, A. Bazin, B. Kuyken, R. Baets, and D. Van Thourhout, arXiv preprint arXiv:1508.06318 (2015).
[27] C. Wolff, P. Gutsche, M. J. Steel, B. J. Eggleton, and C. G. Poulton, arXiv preprint arXiv:1508.02458 (2015), arXiv:1508.02458.
[28] G. P. Agrawal, *Nonlinear fiber optics* (Academic press, 2007).
[29] T. Barwicz and H. A. Haus, Journal of lightwave technology **23**, 2719 (2005).
[30] P. Dong, W. Qian, S. Liao, H. Liang, C.-C. Kung, N.-N. Feng, R. Shafiiha, J. Fong, D. Feng, A. V. Krishnamoorthy, *et al.*, Optics express **18**, 14474 (2010).
[31] R. Claps, V. Raghunathan, D. Dimitropoulos, and B. Jalali, Opt. Express **12**, 2774 (2004).